Molecular Layer Deposition Using Ring-Opening Reactions : Molecular Modeling of the Film Growth and the Effects of Hydrogen Peroxide

Keskivali, Laura

2018-07

Keskivali , L , Putkonen , M , Puhakka , E , Kenttä , E , Kint , J , Ramachandra , R K , Detavernier , C & Simell , P 2018 , ' Molecular Layer Deposition Using Ring-Opening Reactions : Molecular Modeling of the Film Growth and the Effects of Hydrogen Peroxide ' , ACS Omega , vol. 3 , no. 7 , pp. 7141-7149 . https://doi.org/10.1021/acsomega.8b01301 , https://doi.org/10.1021/acs

http://hdl.handle.net/10138/238063
https://doi.org/10.1021/acsomega.8b01301

other
publishedVersion

ACS OMEGA

Article

Cite This: ACS Omega 2018, 3, 7141−7149

Molecular Layer Deposition Using Ring-Opening Reactions: Molecular Modeling of the Film Growth and the Effects of Hydrogen Peroxide

Laura Keskiväli,*[,†] Matti Putkonen,[†] Eini Puhakka,[‡] Eija Kenttä,[†] Jeroen Kint,[§] Ranjith K. Ramachandran,[§] Christophe Detavernier,[§] and Pekka Simell[†]

[†]VTT Technical Research Centre of Finland, P.O. Box 1000, 02044 Espoo, Finland

[‡]Department of Chemistry, University of Helsinki, P.O. Box 55, FI-00014 Helsinki, Finland

[§]Department of Solid State Sciences, Ghent University, Krijgslaan 281/S1, B-9000 Gent, Belgium

Supporting Information

ABSTRACT: Novel coating materials are constantly needed for current and future applications in the area of microelectronics, biocompatible materials, and energy-related devices. Molecular layer deposition (MLD) is answering this cry and is an increasingly important coating method for organic and hybrid organic−inorganic thin films. In this study, we have focused on hybrid inorganic−organic coatings, based on trimethylaluminum, monofunctional aromatic precursors, and ring-opening reactions with ozone. We present the MLD processes, where the films are produced with trimethylaluminum, one of the three aromatic precursors (phenol, 3-(trifluoromethyl)phenol, and 2-fluoro-4-(trifluoromethyl)-benzaldehyde), ozone, and the fourth precursor, hydrogen peroxide. According to the in situ Fourier-transform infrared spectroscopy measurements, the hydrogen peroxide reacts with the surface carboxylic acid group, forming a peroxyacid structure (C(O)−O−OH), in the case of all three processes. In addition, molecular modeling for the processes with three different aromatic precursors was carried out. When combining these modeling results with the experimental research data, new interesting aspects of the film growth, reactions, and properties are exploited.

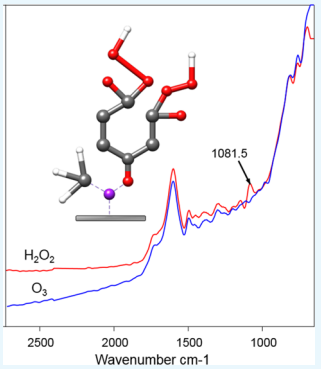

INTRODUCTION

A growing interest towards organic and hybrid inorganic−organic nanomaterials has accelerated the development of various thin film materials produced by molecular layer deposition (MLD) techniques.[1−3] As a variation of atomic layer deposition (ALD), the MLD technique produces thin films from precursor gases by one atomic or molecular layer at a time. The principles of the technique are the same as for ALD, as the films are formed by sequential, self-limiting surface reactions.[1,3,4] Compared to purely inorganic materials, the advantages of organic and hybrid materials lie in their altered mechanical and physical properties, such as flexibility and optical or thermal properties. The tailored properties of MLD films enable the development of novel applications for technical challenges in catalysis,[5] energy storage,[6] biomedical materials,[7] and microelectronics.[8,9]

Sufficient vapor pressure of the precursor is a lifeline for feasible ALD and MLD processes. With high molecular weight organic compounds, the vapor pressure is often readily too low, causing difficulties in MLD processes.[10,11] In general, the more the functionalities and the bigger the compound, the lower the vapor pressure. In addition, organic compounds and materials do not tolerate high temperatures (>150 °C) due to facile decomposition, the reason for which the deposition temperatures for MLD films are often restricted. Thus, finding precursors for novel MLD processes with proper temperature properties is time consuming. Therefore, the ring-opening reaction is an intriguing approach for enabling the new MLD thin film materials.[12−14]

In addition to discovering novel MLD precursors, the modification of existing processes and materials can be beneficial for various applications. The modification can be achieved with chemical or physical treatments of the produced film, or with additional precursors altering the film's growth and properties during the process. For example, the effects of hydrogen peroxide as an extra precursor or an alternative oxidizing agent in the MLD process can produce novel properties for the coatings. Traditional oxidants and oxygen sources in ALD and MLD are ozone, O_2 plasma, and water. It has been demonstrated that, for example, Al_2O_3 deposited by using TMA + H_2O_2 is denser and the monolayer growth initiates faster than the films deposited by using H_2O as an oxygen source.[15,16] H_2O_2 has been used scarcely as an oxidizer for ALD processes, but hardly ever for MLD with organic precursors.[17,18]

Different molecular modeling techniques can be used to support experimental characterization of thin film structures and

Received: June 11, 2018
Accepted: June 21, 2018
Published: July 2, 2018

DOI: 10.1021/acsomega.8b01301
ACS Omega 2018, 3, 7141−7149

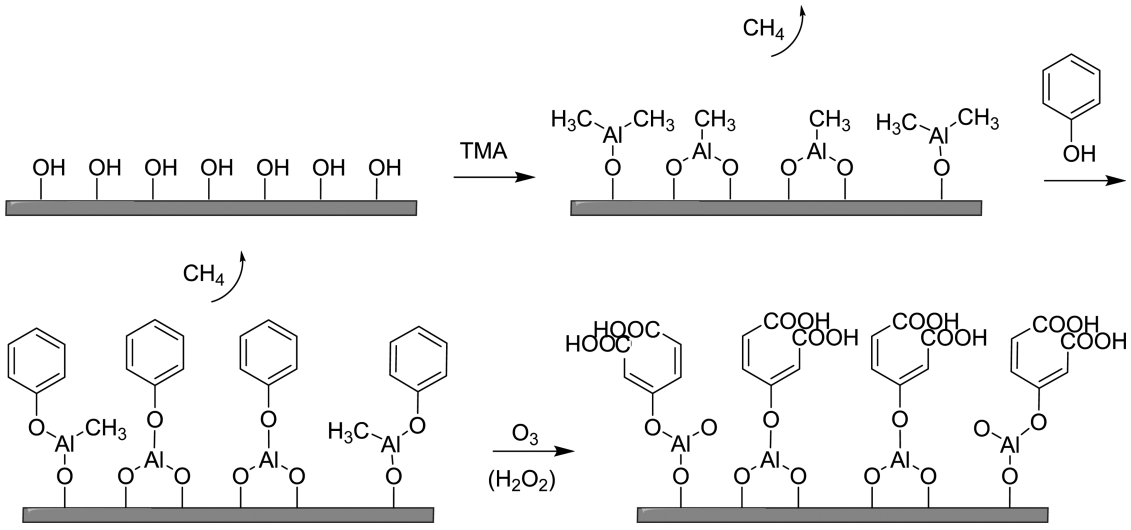

Figure 1. Suggested reactions during one cycle in the TMA + phenol + O_3(+H_2O_2) process. Figure is reconstructed from ref 14.

to gain further insight into deposition mechanisms. Density functional theory (DFT)-based DMol3 and Turbomole calculations have been used to study the functionalization of carbon nanotubes via TMA cycles.[19] The dissociative reaction of mono(alkylamino)silane precursors on a hydroxylated SiO_2(001) surface has also been investigated at the DFT level using the Vienna ab initio simulation package (VASP) simulations.[20] Kinetic Monte Carlo simulations have been used to describe the ALD film growth of HfO_2.[21] In the present study, DFT methods were utilized to study the growth of the MLD layers step by step at the atomic level.

Previously, we presented novel MLD processes with monofunctional aromatic precursors, when TMA, one of the three aromatic compounds (phenol, 3-(trifluoromethyl)phenol, and 2-fluoro-4-(trifluoromethyl)benzaldehyde) and ozone were utilized in the three-step MLD process.[14] The processes were carried out at low temperatures (75−100 °C), and the ALD-type film growth was achieved. Furthermore, we demonstrated the ring-opening reaction between the aromatic ring and ozone, which introduced new functional groups on the film surface, thus, enabling the continuous film growth (Figure 1). However, despite the inclusive analysis and characterization of the films and processes, questions related to the growth mechanisms and properties remained. In this work, we utilized DFT modeling for studying growth mechanisms for all three processes (TMA + phenol + O_3, TMA + 3-(trifluoromethyl)phenol + O_3, and TMA + 2-fluoro-4-(trifluoromethyl)benzaldehyde + O_3). In addition, in previous studies the role of the hydrogen peroxide remained unclear. Therefore, we also present the in situ Fourier-transform infrared spectroscopy (FTIR) data for processes utilizing hydrogen peroxide.

RESULTS AND DISCUSSION

In Situ FTIR Characterization. The in situ FTIR spectra measured after the TMA, aromatic precursor, and ozone pulses were similar to the spectra obtained during earlier studies with the same MLD tool and coupled in situ FTIR system.[14] Because of the similarity, we can conclude that the MLD tool and connected in situ FTIR system worked correspondingly to the previous study. Before the experiment, we expected the effect of hydrogen peroxide to be relatively minor, because as presented in Figure 1, the opening of the aromatic ring and the formation of the carboxylic acid end groups are already taking place with O_3.

According to the literature, the reaction between carboxylic acid and hydrogen peroxide produces a peroxide structure i.e., peroxy acids (C(O)−O−OH).[25,26] This structure is seen in the spectra (Figures 2−4) as a band with a wavenumber of 1082

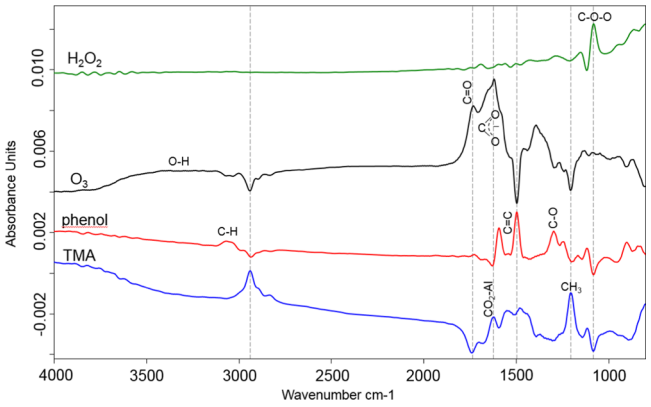

Figure 2. In situ FTIR averaged out difference spectra after 200 cycles of TMA + phenol + O_3 + H_2O_2 pulses at 100 °C onto a Si-wafer.

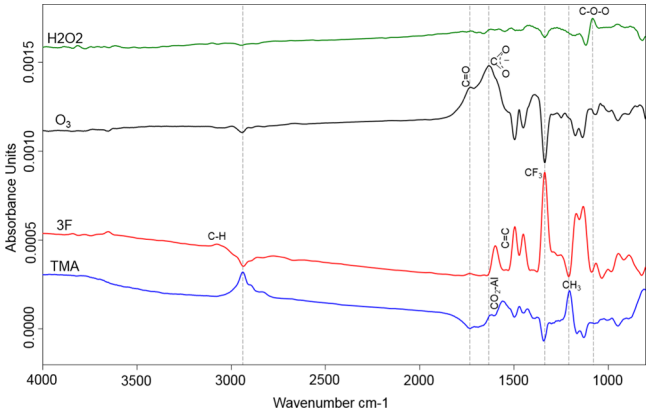

Figure 3. In situ FTIR averaged out difference spectra after 200 cycles of TMA + 3F + O_3 + H_2O_2 pulses at 100 °C onto a Si-wafer.

DOI: 10.1021/acsomega.8b01301
ACS Omega 2018, 3, 7141−7149

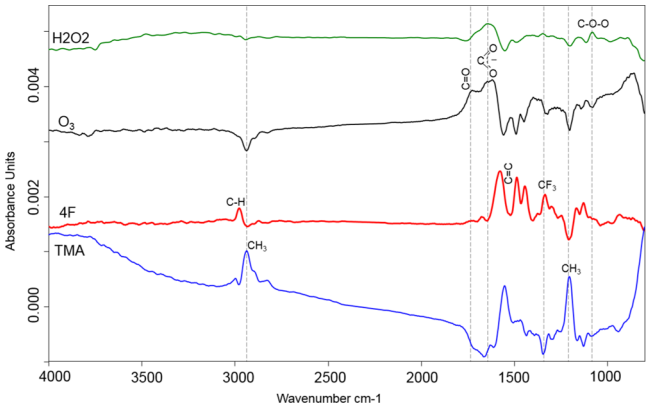

Figure 4. In situ FTIR averaged out difference spectra after 200 cycles of TMA + 4F + O_3 + H_2O_2 pulses at 100 °C onto a Si-wafer.

cm^{-1}, (C−O−OH).[27,28] This band is the strongest in the spectrum of phenol process, but can be detected with the two other precursors (3F and 4F) as well.

Since no new bands are seen in the difference spectra after the H_2O_2 pulse, we conclude that the peroxyacid is the only new structure formed during the H_2O_2 pulse. Furthermore, due to the lack of negative absorbance in the spectra, it can be stated that the carbonyl group (C═O) stretching vibration from carboxylic acid and carboxylate ion (CO^{2-}) bands (1726, 1610, and 1465−1590 cm^{-1}) still exist on the film surface, as well as the OH-stretching (3200−3765 cm^{-1}) from carboxylic acid. The difference in the remaining chain structures between the carboxylic acid and peroxyacid causes a sift of the band in the area of 1500−1800 cm^{-1}. Although the carbonyl group itself is the same in both structures, the formed peroxyacid structure has different conjugation and dipole moment compared with the carboxylic acid. This difference shifts the band to a slightly lower wavelength (from 1734 to the 1678 cm^{-1}) (Supporting Information, Figure S1).

The investigated aromatic precursors differ from each other with a molecular structure and atomic composition. Fluorine atoms in 3F and 4F molecules are presumably causing variations in the reactions and structures. For this reason, we wanted to study these molecules in detail as well, with both in situ FTIR and DFT modeling. In the case of the 4F process (Figure 4), the carbonyl group (C═O) stretching vibration from carboxylic acid and carboxylate ion (CO^{2-}) bands (1726, 1610, and 1465−1590 cm^{-1}) still exists on the film surface after the hydrogen peroxide pulse, even when averaging and subtraction has been done. This is probably due to the unsaturated reactions during the ozone pulse and the formation of carboxylic acids during the H_2O_2 pulse. The unsaturated reactions in the 4F process can result from the variations in the ring opening and rearrangement of the surface structure. According to the modeling results, the backbonding of the carboxylic acid to the surface is different between the processes, and this can cause variations in the reactions with surface groups and H_2O_2. In the case of phenol (Figure 8) and 3F (Figure 9), hydrogen peroxide can react with the surface carboxyl groups and form the peroxyacid group (C(O)−O−OH). In the case of 4F (Figure 11), the hydrogen peroxide does not react presumably with the remaining C(O)−F group. Even after the possible cleavage of chemical species (such as trifluoropyruvic acid in Figure 12), because of the ozone pulse, the C(O)−F group remains at the surface. These variations between all three processes are seen with changing absorbance in the H_2O_2 spectra.

The formed peroxyacid structure is adequately stable to react with the next TMA pulse, thus, enabling the continuous film growth. According to the in situ FTIR results, the reaction between the CH_3 group (TMA) and the OH group is similar to the carboxylic acid and peroxyacid. The kinetics of the backbonding of carboxylic acid to the surface in relation to the next H_2O_2 pulse needs further studying. Rearrangement of the surface can occur before the H_2O_2 pulse, or these events (backbonding and formation of the peroxyacid) can overlap.

Molecular Modeling. In the present study, molecular modeling was also utilized to characterize the formation of the

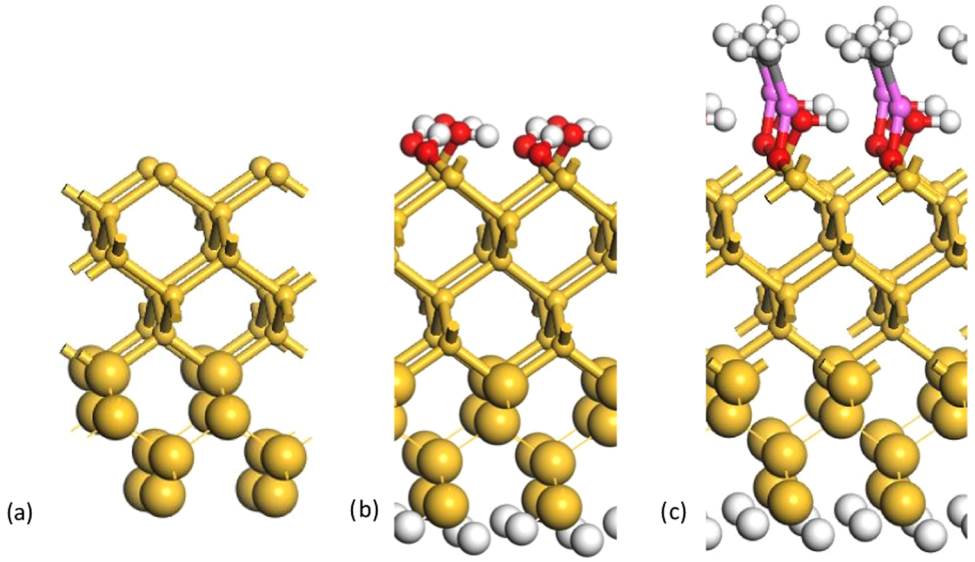

Figure 5. Silica (100) substrate. (a) Nonhydroxylated surface. (b) The hydroxylated surface where two hydroxyl groups are connected to each Si atom. (c) Al−CH_3 groups deposited onto the hydroxylated surface. Ball-and-stick model: atoms were included for geometry optimization. van der Waals spheres: atoms had constant positions during the geometry optimization. Yellow: silicon, red: oxygen, white: hydrogen, pink: aluminum, and gray: carbon.

DOI: 10.1021/acsomega.8b01301
ACS Omega 2018, 3, 7141−7149

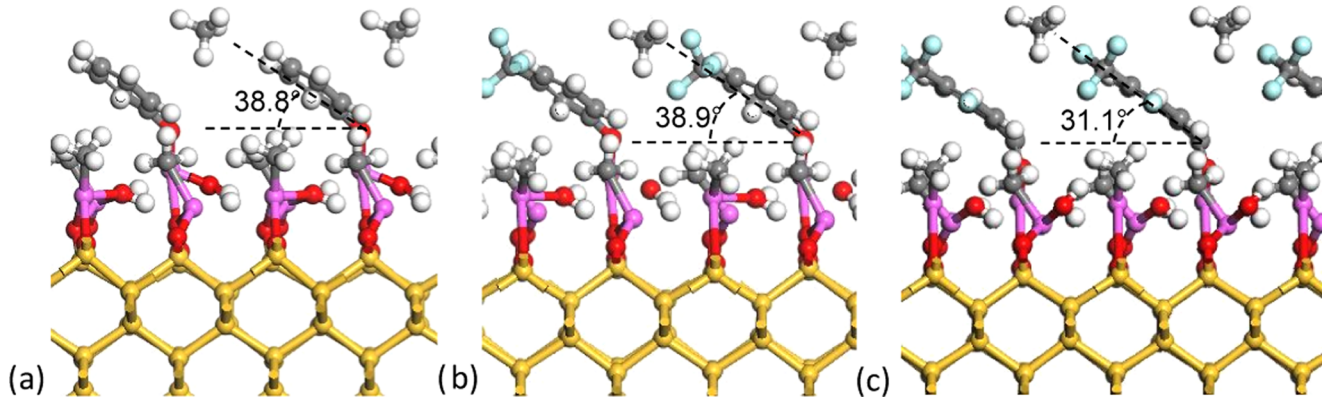

Figure 6. Aromatic precursors on the Al−CH_3 covered silica substrate. (a) Phenol, (b) 3F, and (c) 4F. Yellow: silicon, pink: aluminum, red: oxygen, gray: carbon, white: hydrogen, and light blue: fluorine.

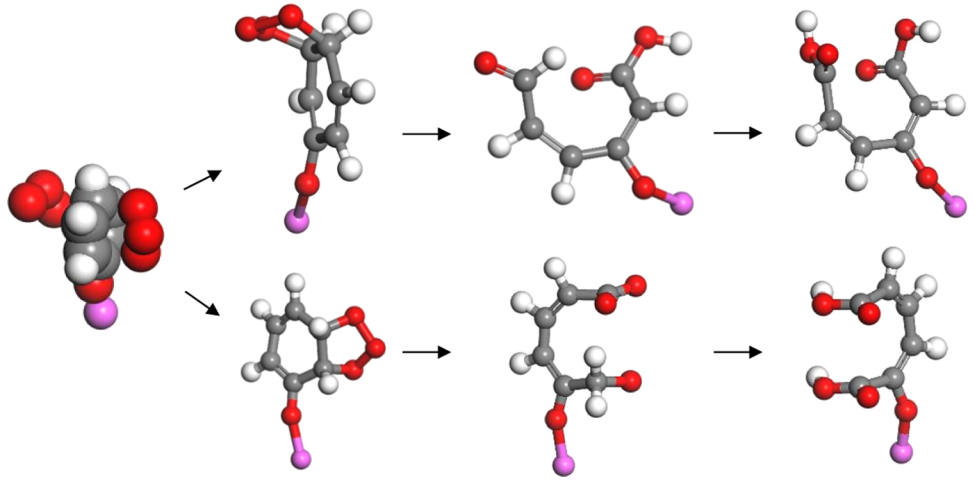

Figure 7. The opening mechanisms of the phenol on the substrate surface in the presence of ozone. Above: the C3−C4 opening. Below: the C2−C3 opening. Pink: aluminum, red: oxygen, gray: carbon, and white: hydrogen.

MLD layers and to assist the interpretation of the experimental findings. The focus was on the functional groups of the surface and their role in the growth process of the MLD layers. The study was started by generating the (100) surface of the silica substrate from the optimized unit cell of cubic SiO_2, the lattice parameters of which are $a = b = c = 0.539$ nm and $\alpha = \beta = \gamma = 90.0°$. The thickness of the generated surface was 1.07 nm (nine Si atom layers), and the positions of the uppermost Si atoms (a thickness of 0.54 nm) were allowed to relax (Figure 5a). To describe the surface structure as realistic as possible and to obtain a surface model for the silica (100) substrate, the surface was covered with hydroxyl groups, so that each Si atoms had two hydroxyl groups. The charge neutrality of the structure was obtained by adding H atoms onto the Si atoms at the bottom of the surface model. The surface structure was reoptimized (Figure 5b), and this model was used as a surface model for the deposition studies of precursors. In all calculated cases, the positions of the bottommost Si atoms of the substrate were kept constant during the optimizing of the MLD layer.

The deposition of the MLD layer starts with a TMA pulse. As a result, an aluminum−methyl (Al−CH_3) group-covered layer structure was obtained that is also detected through in situ FTIR spectra (Figures 2−4). To obtain the maximum coverage of Al−CH_3 groups (one group per 0.15 nm^2) onto the silica (100) surface, the Al−CH_3 group has to be deposited on each Si atoms. On the basis of this, half of the hydroxyl groups were replaced with Al−CH_3 groups, and half of the hydroxyl groups were kept on the substrate surface (Figure 5c).

During the next pulse, the aromatic compound (phenol, 3F or 4F) reacts with methyl (CH_3) groups, and methane desorbs from the substrate surface. It is known that aromatic compounds favor a tilted bonding geometry towards the substrate of approximately 35° in the case of polyurea.[29] In this case, the bonding angle varies between 31 and 39° being the smallest for 4F. This means that only one aromatic compound can settle on the area of 0.58 nm^2 (Figure 6). On this area, there are originally four methyl groups, and the adsorption of aromatic compounds removes one methyl group from the surface in the form of methane. As a consequence of the self-organizing of the Si−O−Al coordination structure, it is possible that a part of the remaining methyl group may also desorb from the surface at this stage. However, in our molecular modeling study, it was supposed that the methyl groups desorb as methane from the surface during the next ozone pulse. In these studies, the surface was covered with ozone molecules, and each methyl group was removed as methane from the surface step by step. Ozone molecules were allowed to participate in the self-organizing of the Si−O−Al surface structure. After the desorption of methyl groups, differences were detected in the coordination geometry of Al atoms. In the case of phenol, the surface Al atoms reach energetically stable structures as a three-coordinated form, but

DOI: 10.1021/acsomega.8b01301
ACS Omega 2018, 3, 7141−7149

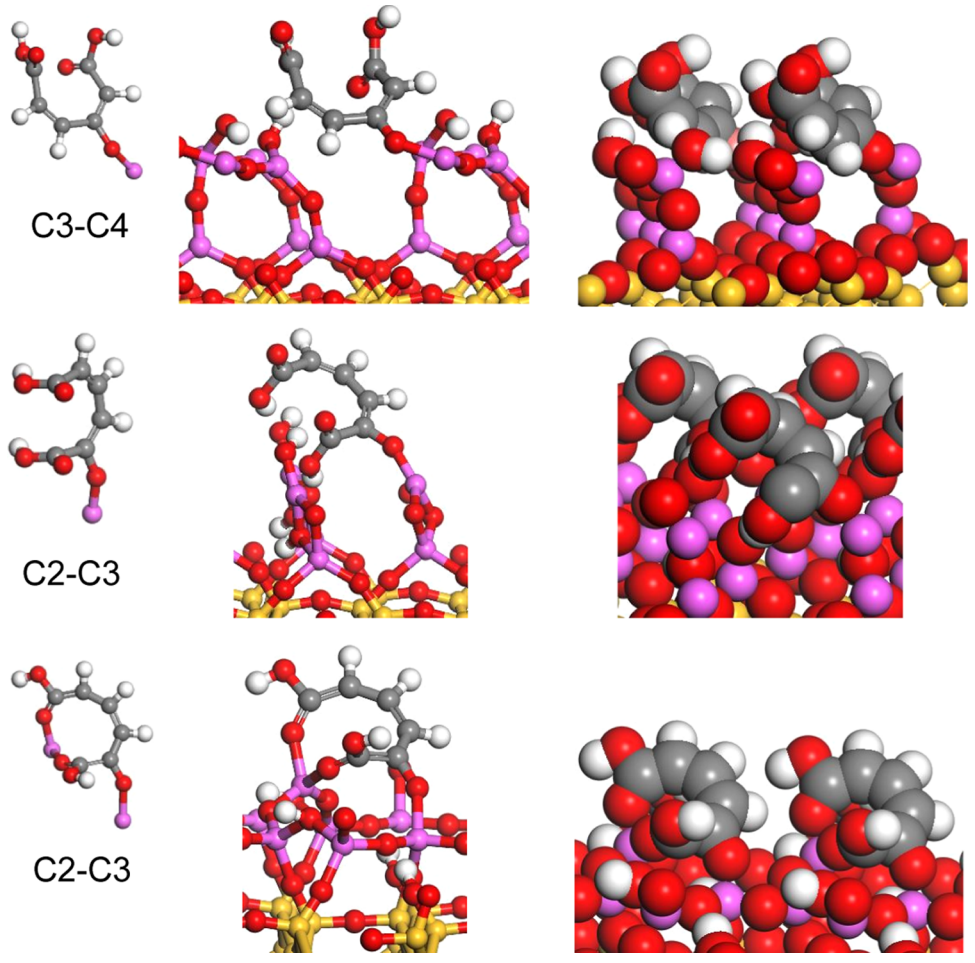

Figure 8. The MLD layer formed with the C3−C4 (above) and C2−C3 (middle and below) openings of phenol. Yellow: silicon, pink: aluminum, red: oxygen, gray: carbon, and white: hydrogen.

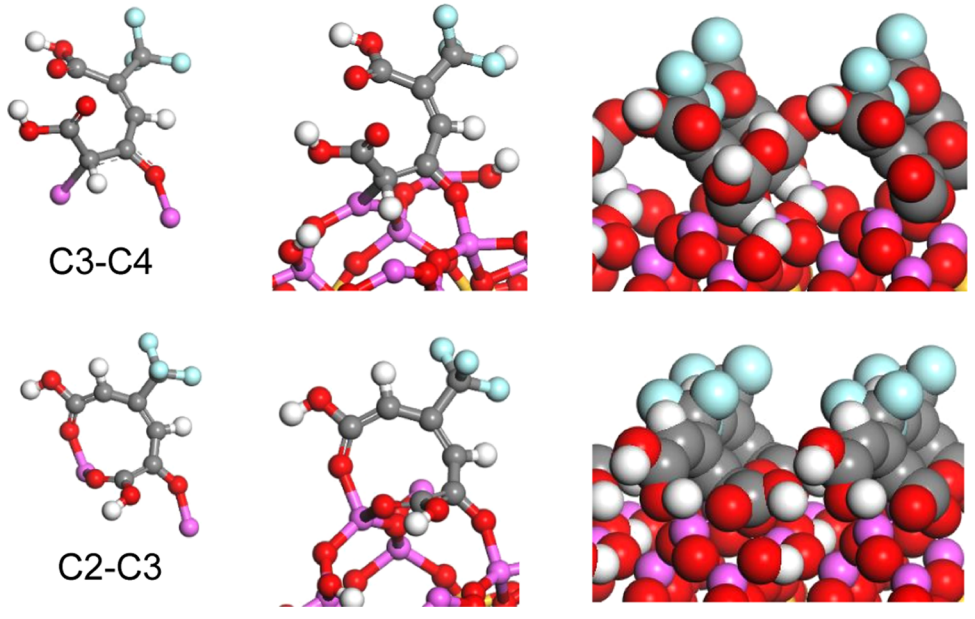

Figure 9. The MLD layer formed with the C3−C4 (above) and C2−C3 (below) openings of 3F. Pink: aluminum, red: oxygen, gray: carbon, white: hydrogen, and light blue: fluorine.

those of 3F and 4F appear as four-coordinated complexes (Figure S2).

During the ozone pulse, the opening of the aromatic rings occurs, which leads to the formation of carbonyl and carboxyl groups. In the case of phenol, two ring-opening mechanisms are

DOI: 10.1021/acsomega.8b01301
ACS Omega 2018, 3, 7141−7149

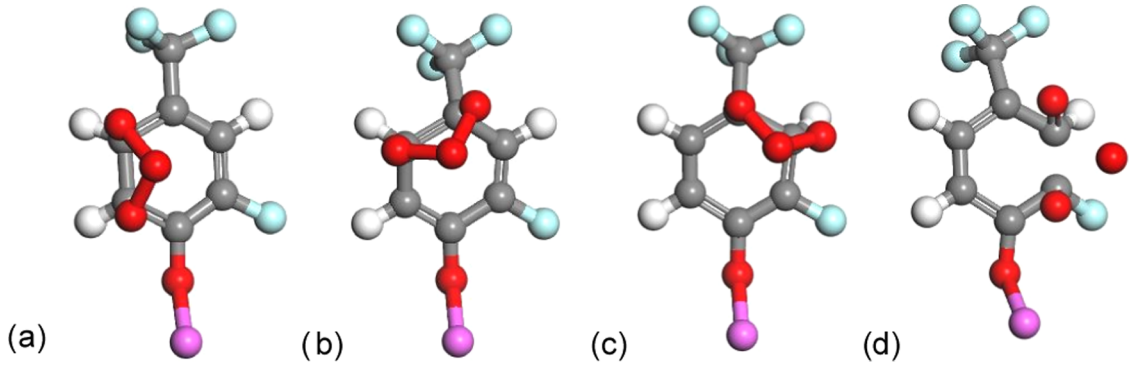

Figure 10. The investigated opening mechanisms of 4F on the substrate surface in the presence of ozone, and their relative energies calculated using the surface models: (a) 0.00 eV, (b) 0.21 eV, (c) 0.14 eV, and (d) −1.54 eV. Pink: aluminum, red: oxygen, gray: carbon, white: hydrogen, and light blue: fluorine.

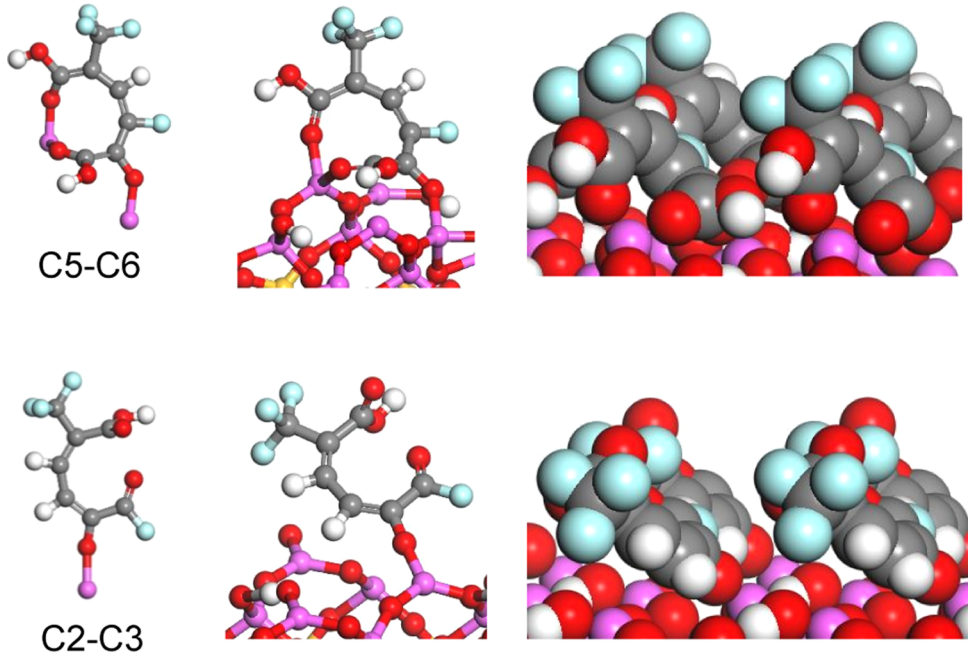

Figure 11. The MLD layer formed with the C5−C6 (above) and C2−C3 (below) openings of 4F. Pink: aluminum, red: oxygen, gray: carbon, white: hydrogen, and light blue: fluorine.

considered, opening between the C2 and C3 carbons, and the C3 and C4 carbons (Figure 7). When the surface Al atoms are three-coordinated, the C2−C3 opening leads to a 0.24 eV energetically more stable surface structure than the C3−C4 opening. If self-organizing of the Si−O−Al surface structure has proceeded from the three-coordinated Al atoms to the four-coordinated Al atoms, the C2−C3 opening leads to an even more stable structure (2.64 eV) than the corresponding structure with the three-coordinated Al atoms. The back-bonding of carboxyl groups of the ring-opened phenol to the surface Al atoms is the possible explanation for this (Figure 8). After the ring opening of the phenol, the bonding angle of the surface species is approximately 50°.

In the case of 3F, the C2−C3 and C3−C4 ring openings were also considered. In both of the surface complexes, the Al atoms are four-coordinated. Of these complexes, the C2−C3 opening is 1.87 eV energetically more favorable, because of the backbonding of the carboxyl groups to the surface Al atoms, as in the case of phenol (Figure 9). However, without backbonding, the carboxyl groups are more easily available for the reactions of the next pulse. The bonding angles of the surface species are about 59 and 68°, respectively in the C3−C4 and C2−C3 opening products.

In the case of 4F, four different ring-opening mechanisms, C5−C6 (Figure 10a), C4−C5 (Figure 10b), C3−C4 (Figure 10c), and C2−C3 (Figure 10d) were investigated. When the optimized structures for different 4F-ozone complexes were determined, the C5−C6 coordinated structure was detected to be energetically more favorable than C3−C4 and C4−C5 structures, but the C5−C6 structure is still significantly less stable than the C2−C3 structure, whose ring opening occurs spontaneously. Its energy is 1.54 eV more favorable than that of the C5−C6 structure without opening.

In addition to the C2−C3 ring opening, the C5−C6 opening was also determined. The geometry optimized structure indicates that the backbonding occurs via the carboxyl groups onto the surface Al atoms (Figure 11) in the case of C5−C6 opening, but not during the C2−C3 opening. Therefore, the final C2−C3 structure is 1.97 eV less stable than the C5−C6 structure.

DOI: 10.1021/acsomega.8b01301
ACS Omega 2018, 3, 7141−7149

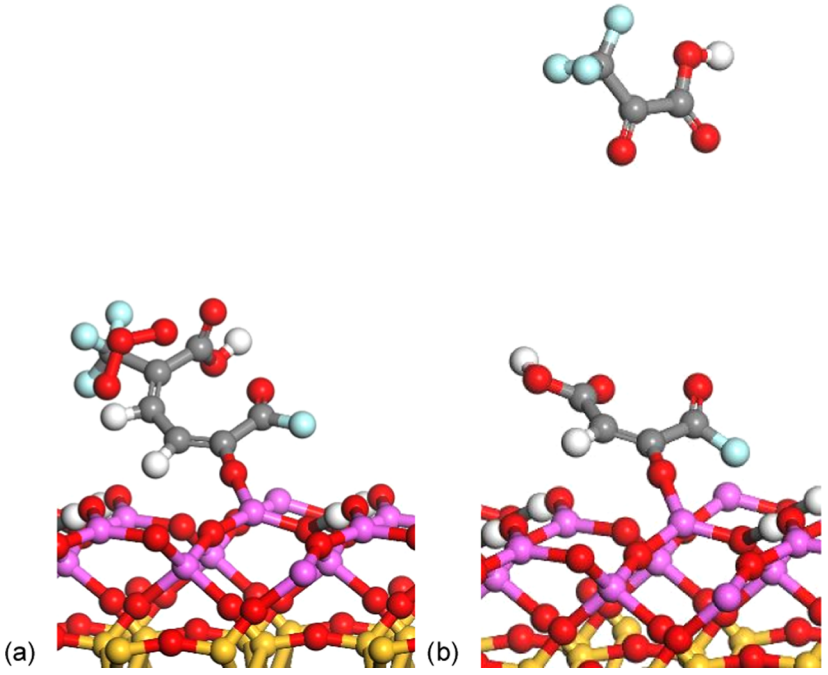

Figure 12. The MLD layer formed with the C2−C3 opening (a) without and (b) with the C4−C5 cleavage of 4F. Pink: aluminum, red: oxygen, gray: carbon, white: hydrogen, and light blue: fluorine.

In the experiments, the diminishing amount of fluorine on the MLD layer was detected in the case of 4F precursors compared with the 3F case, through the original amount of fluorine in the precursor. Therefore, the second bond cleavage after the initial aromatic ring opening was also taken into account. It was supposed that after the ozone pulse, trifluoropyruvic acid ($CF_3COCOOH$) is released from the 4F species (Figure 12). The release can occur either in the case of the C2−C3 or C5−C6 ring opening. Energetically, the release of trifluoropyruvic acid is a very favorable reaction, because in the case of the C2−C3 opening, the energy released is −6.59 eV. The result corresponds to the experimental findings on the chemical composition of the MLD layers.[14] Chemical compositions and atomic ratios of the investigated MLD surfaces after the first MLD cycle are presented in Table 1.

Modeling also explains the differences between the contact angles in the previous study.[14] With the most favorable cleavage in the case of 4F, the cleavage of the C5−C6 and backbonding of the carboxylic acid to the surface structure lead to the surface, where the CF_3 group and one fluorine atom point perpendicularly to the surface, causing the lower surface energy, more hydrophobic surface, and higher contact angle compared with the 3F process.[30,31] In the case of 3F, there is the CF_3 group, but the additional fluorine atom is missing. Furthermore, the hydroxyl group enhances the hydrophilicity and lowers the contact angle. In the case of phenol, there is no fluorine atoms or CF_3 groups, but the longer carbon chain balances the situation with the 3F process.

Table 1. Chemical Compositions and Atomic Ratios of the MLD Layers after the First MLD Cycle According to the Molecular Modeling Results

Chemical Composition (%)	Al	O	H	C	F	Total
TMA + phenol + O_3	10	39	36	15	0	100
TMA + 3F + O_3	10	36	31	16	7	100
TMA + 4F + O_3	10	36	28	16	10	100
TMA + 4F + O_3 − (CCF_3CH)	11	43	32	11	3	100
Atomic Ratio (%)	**Al/O**	**Al/C**	**C/H**	**F/C**		
TMA + phenol + O_3	0.27	0.67	0.42			
TMA + 3F + O_3	0.27	0.57	0.53	0.42		
TMA + 4F + O_3	0.27	0.57	0.58	0.57		
TMA + 4F + O_3 − (CCF_3CH)	0.27	1.00	0.36	0.25		

CONCLUSIONS

In this study, we clarified the role of hydrogen peroxide in four-step MLD processes with TMA, various aromatic precursors, ozone, and H_2O_2. We demonstrated peroxyacid formation in the reaction between carboxylic acid and hydrogen peroxide and continuation of the film growth in all three MLD processes. According to the in situ FTIR measurements, the same peroxyacid structure was formed in the case of phenol, 3-(trifluoromethyl)phenol, and 2-fluoro-4-(trifluoromethyl)-benzaldehyde, at 100 °C.

To obtain the molecular level view of the growth of the MLD layers, we utilized molecular modeling to describe the growth of the MLD layer step by step. As a result, chemical compositions and atomic ratios of different MLD layers were obtained. In these studies, the ring-opening mechanism of aromatic precursors in the presence of ozone was also considered. The results are consistent with the experimental characterization, and nicely explain the differences between the detected contact angles.

These results enable the further development of versatile MLD processes for future materials and applications. However, the relation between the experimental and modeling results needs further studying, because, for example, the probability and kinetics of ring opening and backbonding during the deposition process are still unclear.

DOI: 10.1021/acsomega.8b01301
ACS Omega 2018, 3, 7141−7149

EXPERIMENTAL SECTION AND THEORY OF MODELING

Deposition Processes and in Situ FTIR Measurements. A home-built MLD tool was connected to FTIR measurement equipment (Bruker Tensor 27, globar mid-IR source and KBr beamsplitter, Germany). Si wafers (100) were used as substrates. Four-step (ABCD) processes were constructed from TMA (99.999% SAFC), ozone (generated by a IN USA, Inc. ozone generator from 99.99% O_2), hydrogen peroxide (50 wt % in water, Sigma-Aldrich), and aromatic precursors including phenol (>96% Sigma-Aldrich), 3-(trifluoromethyl)phenol (99% Sigma-Aldrich) (3F), and 2-fluoro-4-(trifluoromethyl)-benzaldehyde (98% Sigma-Aldrich) (4F). TMA was evaporated at room temperature and held in a metallic container. Phenol and 3F were evaporated at 80 °C and 4F at 60 °C. An in situ FTIR measurement was carried out after every precursor pulse. For each of the three processes, 150 cycles were deposited at 100 °C. No carrier gas was used.

Molecular Modeling. Molecular modeling methods based on density functional theory (DFT) were used to generate the structure of the silica (100) substrate and to investigate the formation of MLD layers from monofunctional aromatic precursors via ring-opening reactions using phenol, 3F, and 4F together with TMA and ozone (O_3). The calculations were performed with the CAmbridge Serial Total Energy Package (CASTEP)[22] code implemented into Materials Studio version 8.0 (Dassault Systèmes).[23] The modeling is based on solving the total electronic energy and overall electronic density distribution to define the energetically stable structures.[24] The exchange–correlation was described with generalized gradient approximation Perdew–Burke–Ernzerhof. As a compromise between the accuracy and computational time of calculations, the ultrasoft pseudopotentials were used for each element. The used potentials were Al_00PBE.usp for aluminum, C_00PBE.usp for carbon, F_00PBE.usp for fluorine, H_00PBE.usp for hydrogen, O_soft00.usp for oxygen, and Si_soft00.usp for silicon. The kinetic cut-off energy for a plane wave expansion of the wave function was 300 eV.

ASSOCIATED CONTENT

Supporting Information

The Supporting Information is available free of charge on the ACS Publications website at DOI: 10.1021/acsomega.8b01301.

More detailed information of the in situ FTIR measurements and the formation of peroxyacid structure, modeling of the surface structure of the deposited film (PDF)

AUTHOR INFORMATION

Corresponding Author

*E-mail: laura.keskivali@vtt.fi.

ORCID

Laura Keskiväli: 0000-0002-6920-8243

Author Contributions

This manuscript was written through contributions of all authors. All authors have given approval to the final version of the manuscript.

Notes

The authors declare no competing financial interest.

ACKNOWLEDGMENTS

This research was supported by the Academy of Finland (project ID 288212). Part of the work was carried out within the framework of the COST Action MP1402 – Hooking together European research in Atomic Layer Deposition (HERALD).

REFERENCES

(1) Yoshimura, T.; Tatsuura, S.; Sotoyama, W. Polymer Films Formed with Monolayer Growth Steps by Molecular Layer Deposition. *Appl. Phys. Lett.* **1991**, *59*, 482–484.

(2) Putkonen, M.; Harjuoja, J.; Sajavaara, T.; Niinistö, L. Atomic Layer Deposition of Polyimide Thin Films. *J. Mater. Chem.* **2007**, *17*, 664–669.

(3) Du, Y.; George, S. M. Molecular Layer Deposition of Nylon 66 Films Examined Using in Situ FTIR Spectroscopy. *J. Phys. Chem. C* **2007**, *111*, 8509–8517.

(4) Matero, R.; Rahtu, A.; Ritala, M.; Leskelä, M.; Sajavaara, T. Effect of Water Dose on the Atomic Layer Deposition Rate of Oxide Thin Films. *Thin Solid Films* **2000**, *368*, 1–7.

(5) Sarkar, D.; Ishchuk, S.; Taffa, D. H.; Kaynan, N.; Berke, B. A.; Bendikov, T.; Yerushalmi, R. Oxygen-Deficient Titania with Adjustable Band Positions and Defects; Molecular Layer Deposition of Hybrid Organic-Inorganic Thin Films as Precursors for Enhanced Photocatalysis. *J. Phys. Chem. C* **2016**, *120*, 3853–3862.

(6) Piper, D. M.; Travis, J. J.; Young, M.; Son, S. B.; Kim, S. C.; Oh, K. H.; George, S. M.; Ban, C.; Lee, S. H. Reversible High-Capacity Si Nanocomposite Anodes for Lithium-Ion Batteries Enabled by Molecular Layer Deposition. *Adv. Mater.* **2014**, *26*, 1596–1601.

(7) Momtazi, L.; Sønsteby, H. H.; Dartt, D. A.; Eidet, J. R.; Nilsen, O. Bioactive Titaminates from Molecular Layer Deposition. *RSC Adv.* **2017**, *7*, 20900–20907.

(8) Zhou, H.; Bent, S. F. Molecular Layer Deposition of Functional Thin Films for Advanced Lithographic Patterning. *ACS Appl. Mater. Interfaces* **2011**, *3*, 505–511.

(9) Ban, C.; George, S. M. Molecular Layer Deposition for Surface Modification of Lithium-Ion Battery Electrodes. *Adv. Mater. Interfaces* **2016**, *3*, No. 1600762.

(10) Sundberg, P.; Karppinen, M. Organic and Inorganic-Organic Thin Film Structures by Molecular Layer Deposition: A Review. *Beilstein J. Nanotechnol.* **2014**, *5*, 1104–1136.

(11) George, S. M. Atomic Layer Deposition: An Overview. *Chem. Rev.* **2010**, *110*, 111–131.

(12) George, S. M.; Yoon, B.; Dameron, A. Surface Chemistry for Molecular Layer Deposition of Organic and Hybrid Organic-Inorganic Polymers. *Acc. Chem. Res.* **2009**, *42*, 498–508.

(13) Adamczyk, N. M.; Dameron, A. A.; George, S. M. Molecular Layer Deposition of Poly(p-Phenylene Terephthalamide) Films Using Terephthaloyl Chloride and P-Phenylenediamine. *Langmuir* **2008**, *24*, 2081–2089.

(14) Svärd, L. K. K.; Putkonen, M.; Kenttä, E.; Sajavaara, T.; Krahl, F.; Karppinen, M.; Van de Kerckhove, K.; Detavernier, C.; Simell, P. Low-Temperature Molecular Layer Deposition Using Monofunctional Aromatic Precursors and Ozone-Based Ring-Opening Reactions. *Langmuir* **2017**, *33*, 9657–9665.

(15) Kaufman-Osborn, T.; Chagarov, E. A.; Kummel, A. C. Atomic Imaging and Modeling of H_2O_2(g) Surface Passivation, Functionalization, and Atomic Layer Deposition Nucleation on the Ge(100) Surface. *J. Chem. Phys.* **2014**, *140*, No. 204708, 1–9.

(16) Spiegelman, J.; Alvarez, D.; Holmes, R.; Heinlein, E.; Shamsi, Z. Advantages of Hydrogen Peroxide as an Oxidant for Atomic Layer Deposition and Related Novel Delivery System. *MRS Proc.* **2013**, *1494*, 209–214.

(17) Fan, J.-F.; Sugioka, K.; Toyoda, K. Related Content Low-Temperature Growth of Thin Films of Al_2O_3 by Sequential Surface Chemical Reaction of Trimethylaluminum and H_2O_2. *Jpn. J. Appl. Phys.* **1991**, *30*, L1139–L1141.

DOI: 10.1021/acsomega.8b01301
ACS Omega 2018, 3, 7141–7149

(18) Ritala, M.; Asikainen, T.; Leskelä, M. Enhanced Growth Rate in Atomic Layer Epitaxy of Indium Oxide and Indium-Tin Oxide Thin Films. *Electrochem. Solid-State Lett.* **1998**, *1*, 156−157.
(19) Förster, A. Ab-Initio Studies of Reactions to Functionalize Carbon Nanotubes. Bachelor Thesis; Chemniz University of Technology, 2012.
(20) Huang, L.; Han, B.; Fan, M.; Cheng, H. Design of Efficient Mono-Aminosilane Precursors for Atomic Layer Deposition of SiO_2 Thin Films. *RSC Adv.* **2017**, *7*, 22672−22678.
(21) Shirazi, M.; Elliott, S. D. Atomistic Kinetic Monte Carlo Study of Atomic Layer Deposition Derived from Density Functional Theory. *J. Comput. Chem.* **2014**, *35*, 244−259.
(22) Clark, S. J.; Segall, M. D.; Pickard, C. J.; Hasnip, P. J.; Probert, M. I. J.; Refson, K. First Principles Methods Using CASTEP. *Z. Kristallogr.* **2005**, *220*, 567−570.
(23) Systemes, D. *Materials Studio*; BIOVIA Corp.: San Diego, 2014.
(24) Leach, A. R. *Molecular Modelling, Principles and Applications*, 2nd ed.; Pearson Education Limited: Essex, 2001.
(25) Swern, D. Organic Peracids. *Chem. Rev.* **1949**, *45*, 1−68.
(26) Strukul, G. *Catalytic Oxidations with Hydrogen Peroxide as Oxidant*, 1st ed.; Springer Science & Business Media, Kluwer Academic Publishers: Dordrecht, 1992; pp 76−82.
(27) Socrates, G. *Infrared and Raman Characteristic Group Frequencies: Tables and Charts*, 3rd ed.; Wiley: West Sussex, 2004; pp 130−132.
(28) Pretsch, E.; Buhlmann, P.; Badertscher, M. *Structure Determination of Organic Compounds*, 4th ed.; Springer: Berlin Heidelberg, 2009; p 291.
(29) Park, Y. S.; Choi, S. E.; Kim, H.; Lee, J. S. Fine-Tunable Absorption of Uniformly Aligned Polyurea Thin Films for Optical Filters Using Sequentially Self-Limited Molecular Layer Deposition. *ACS Appl. Mater. Interfaces* **2016**, *8*, 11788−11795.
(30) Butter, R. S.; Waterman, D. R.; Lettington, A. H.; Ramos, R. T.; Fordham, E. J. Production and Wetting Properties of Fluorinated Diamond-like Carbon Coatings. *Thin Solid Films* **1997**, *311*, 107−113.
(31) Nishino, T.; Meguro, M.; Nakamae, K.; Matsushita, M.; Ueda, Y. The Lowest Surface Free Energy Based on $-CF_3$ Alignment. *Langmuir* **1999**, *15*, 4321−4323.

DOI: 10.1021/acsomega.8b01301
ACS Omega 2018, 3, 7141−7149